rangements of phosphine ligands and require passage through several intermediate TTP topologies in order to return to the ground-state arrangement with two eclipsed prismatic phosphines and a capping phosphine on the opposite prismatic face.

**Conclusions**

$^{13}C$ and $^{31}P$ CP/MAS NMR data obtained over a range of temperatures are consistent with a tricapped-trigonal-prismatic structure for $W(PMe_3)_3H_6$, with two phosphine ligands in eclipsed prismatic sites and the third in the opposite capping site. In contrast to the results of previous crystallographic studies on such compounds, the NMR spectra suggest that the two prismatic phosphine ligands in each molecule are slightly inequivalent. At temperatures above ambient, interchange of ligand functionality for the phosphine ligands is observed by magnetization-transfer experiments and, at still higher temperatures, by simulation of the exchange-broadened NMR line shapes observed experimentally. Rate data from the two methods of analysis suggest Arrhenius activation parameters for ligand functionality interchange of $E_a = 148.8 \pm 15$ kJ mol$^{-1}$ and $A = 6.6 \times 10^{23}$ s$^{-1}$. The rate of functionality interchange reaches ca. 2000 Hz by the decomposition point of the material (381 K). A mechanism for this exchange has been proposed, involving the "double rearrangement"

$$\text{TTP(ground state)} \rightleftharpoons \text{MSA} \rightleftharpoons \text{TTP(excited state)} \rightleftharpoons \text{MSA} \rightleftharpoons \text{TTP(ground state)}$$

In this mechanism slight stretches of the polytypal edges result in interchange of ligand functionality without the need for unfavorable spatial permutation of the phosphine ligands.

**Acknowledgment.** J. Pound is thanked for a sample of $W(PMe_3)_3H_6$, and Drs. J. M. Twyman, D. O'Hare, L. L. Wong, and A. Sella are thanked for valuable assistance and advice. The SERC is thanked for financial support.

Contribution from the Departments of Chemistry, University of Minnesota, Minneapolis, Minnesota 55455, and University of New Orleans, New Orleans, Louisiana 70122

# Models for Diiron–Oxo Proteins: The Peroxide Adduct of $Fe_2(HPTB)(OH)(NO_3)_4$

Bridget A. Brennan,† Qiuhao Chen,† Carlos Juarez-Garcia,† Anne E. True,† Charles J. O'Connor,‡ and Lawrence Que, Jr.*,†

*Received October 23, 1990*

The complex of $Fe(NO_3)_3$ and *N,N,N',N'*-tetrakis(2-benzimidazolylmethyl)-2-hydroxy-1,3-diaminopropane (HPTB) is reformulated as $[Fe_2(HPTB)(\mu\text{-}OH)(NO_3)_2](NO_3)_2$ on the basis of $^1H$ NMR, EXAFS, X-ray diffraction, and conductivity data. This complex reacts with hydrogen peroxide to form a 1:1 adduct with a new charge-transfer band at 600 nm ($\epsilon = 1500$ M$^{-1}$ cm$^{-1}$). Resonance Raman studies show two resonance-enhanced vibrations, $\nu_{Fe\text{-}O}$ at 476 cm$^{-1}$ and $\nu_{O\text{-}O}$, which appears as a Fermi doublet centered at 895 cm$^{-1}$; these features shift to 457 and 854 cm$^{-1}$, respectively, with the use of $H_2{}^{18}O_2$ but are not affected by $D_2O$. $^1H$ NMR measurements indicate that the antiferromagnetic coupling is increased from $-J = 20$ cm$^{-1}$ to ca. 70 cm$^{-1}$ upon formation of the peroxide adduct, suggesting the introduction of a new coupling pathway. The $^{57}Fe$ Mössbauer spectrum of the peroxide complex reveals a quadrupole doublet ($\delta = 0.54$ mm/s, $\Delta E_Q = 0.84$ mm/s) distinct from that of the precursor complex ($\delta = 0.49$ mm/s, $\Delta E_Q = 0.66$ mm/s), indicating that the two irons are affected similarly by peroxide binding. Conductivity measurements in $CH_3CN$ show that the adduct is a 1:1 electrolyte. Taken together, the physical data suggest the formulation $[Fe_2(HPTB)(\mu\text{-}\eta^1\text{:}\eta^1\text{-}O_2)(NO_3)_2](NO_3)$ for the peroxide complex. Such dinuclear iron peroxide complexes may be relevant to putative intermediates in the oxygenation of the reduced forms of ribonucleotide reductase and methane monooxygenase.

Diiron centers that are known to interact with dioxygen[1] have been found in hemerythrin,[2] methane monooxygenase,[3,4] and ribonucleotide reductase.[5-7] Deoxyhemerythrin reversibly binds dioxygen and has an active site consisting of a ($\mu$-hydroxo)bis($\mu$-carboxylato)diiron(II) core and five terminal histidines. Dioxygen binds to the diferrous center at the remaining vacant coordination site with concomitant electron and proton transfer, forming a ($\mu$-oxo)diferric center with a coordinated hydroperoxide moiety that is hydrogen-bonded to the oxo bridge (Figure 1).[8,9] Dioxygen may bind in similar or related fashion to the diferrous centers of methane monooxygenase and ribonucleotide reductase to effect the necessary oxidative chemistry associated with these enzymes.[4,10]

Because a number of ligand systems[11-16] have been used successfully to model the spectroscopic and structural properties of the diferric sites in the crystallographically characterized azidomethemerythrin[17] and ribonucleotide reductase,[18] emphasis is now shifting toward efforts that model the diferrous–dioxygen/diferric–peroxide chemistry exhibited by these proteins. While there are a number of examples of structurally characterized dinuclear cobalt and copper peroxide complexes,[19-23] no nonheme diferric peroxide complex is comparably well characterized. Dioxygen adducts of three ferrous complexes are known; that of $[Fe(pyN5)]^{2+}$[24] has only been cursorily characterized,[25] while the adducts of $[Fe|HB(3,5\text{-}i\text{-}Pr_2pz)_3|(OBz)]$[26] and $[Fe_2(N\text{-}Et\text{-}HPTB)OBz]^{2+}$[27] are proposed to have ($\mu$-$\eta^1$,$\eta^1$-peroxo)diiron(III) units on the basis of spectroscopic data. ($\mu$-Peroxo)diiron(III)

† University of Minnesota.
‡ University of New Orleans.

(1) Que, L., Jr.; True, A. E. *Prog. Inorg. Chem.* **1990**, *38*, 97–200.
(2) Klotz, I. M.; Kurtz, D. M., Jr. *Acc. Chem. Res.* **1984**, *17*, 16–22. Sanders-Loehr, J.; Loehr, T. M. *Adv. Inorg. Biochem.* **1979**, *1*, 235–252.
(3) Woodland, M. P.; Patil, D. S.; Cammack, R.; Dalton, H. *Biochim. Biophys. Acta* **1986**, *873*, 237–242.
(4) Fox, B. G.; Froland, W. A.; Dege, J. E.; Lipscomb, J. D. *J. Biol. Chem.* **1989**, *264*, 10023–10033. Fox, B. G.; Surerus, K. K.; Münck, E.; Lipscomb, J. D. *J. Biol. Chem.* **1988**, *263*, 10553–10556.
(5) Reichard, P.; Ehrenberg, A. *Science (Washington, D.C.)* **1983**, *221*, 514–519.
(6) Lynch, J. B.; Juarez-Garcia, C.; Münck, E.; Que, L., Jr. *J. Biol. Chem.* **1989**, *264*, 8091–8096.
(7) Sahlin, M.; Gräslund, A.; Petersson, L.; Ehrenberg, A.; Sjöberg, B.-M. *Biochemistry* **1989**, *28*, 2618–2625.
(8) Shiemke, A. K.; Loehr, T. M.; Sanders-Loehr, J. *J. Am. Chem. Soc.* **1984**, *106*, 4951–4956.
(9) Stenkamp, R. E.; Sieker, L. C.; Jensen, L. H.; McCallum, J. D.; Sanders-Loehr, J. *Proc. Natl. Acad. Sci. U.S.A.* **1985**, 713–716.
(10) (a) Fontecave, M.; Eliason, R.; Reichard, P. *J. Biol. Chem.* **1989**, *264*, 9164–9170. (b) Fontecave, M.; Gerez, C.; Atta, M.; Jeunet, A. *Biochem. Biophys. Res. Commun.* **1990**, *168*, 659–664. (c) Sahlin, M.; Sjöberg, B.-M.; Backes, G.; Loehr, T.; Sanders-Loehr, J. *Biochem. Biophys. Res. Commun.* **1990**, *167*, 813–818.
(11) Armstrong, W. H.; Spool, A.; Papaefthymiou, G. C.; Frankel, R. B.; Lippard, S. J. *J. Am. Chem. Soc.* **1984**, *106*, 3653–3667.
(12) Wieghardt, K.; Pohl, K.; Gebert, K. *Angew. Chem., Int. Ed. Engl.* **1983**, *22*, 727–728.
(13) Toftlund, H.; Murray, K. S.; Zwack, P. R.; Taylor, L. F.; Anderson, O. P. *J. Chem. Soc., Chem. Commun.* **1986**, 191–192.
(14) Gomez-Romero, P.; Casan-Pastor, N.; Ben-Hussein, A.; Jameson, G. B. *J. Am. Chem. Soc.* **1988**, *110*, 1988–1990.

0020-1669/91/1330-1937$02.50/0 

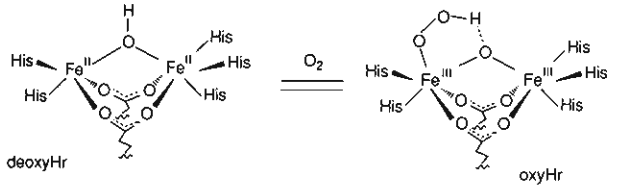


**Figure 1.** Oxygen binding scheme for hemerythrin.

complexes have also been obtained by the addition of $H_2O_2$ to $[Fe(Ph_3PO)_4]^{3+}$[28] and to diferric complexes of dinucleating ligands such as HPTB[29] and 5-Me-HXTA.[30] The only crystallographically characterized iron peroxide complex is $[Fe_6(O)_2(O_2)(O_2CPh)_{12}(OH_2)_2]$,[31] which has a ($\mu_4$-peroxo)tetrairon unit. Our interest in dinuclear iron complexes to model possible intermediates for oxygen activating enzymes such as methane monooxygenase has led us to further characterize the solution structure of the peroxide adduct of $Fe^{III}_2$HPTB, first reported by Nishida.[29]

## Experimental Section

**Synthesis.** The dinucleating ligands HPTB, *N*-Et-HPTB, and 5,6-$Me_2$-HPTB were synthesized by the published procedures.[32,33] Their identity and purity were confirmed by $^1$H NMR spectroscopy.

$Fe_2$(HPTB)(OH)$(NO_3)_4$ was prepared by dissolving HPTB (0.15 g, 0.2 mmol) in 20 mL of EtOH and then adding $Fe(NO_3)_3 \cdot 9H_2O$ (0.20 g, 0.4 mmol).[34] Upon standing, the dark orange solution yielded dark orange needles and platelike crystals. The crystals were washed with EtOH and vacuum-dried to a powdered form for noncrystallographic experiments. The 5,6-$Me_2$-HPTB and *N*-Et-HPTB complexes were synthesized analogously. Anal. Calcd for $Fe_2$(HPTB)(OH)$(NO_3)_4 \cdot 1.5H_2O \cdot 0.5$EtOH, $C_{36}H_{40}Fe_2N_{14}O_{16}$: C, 41.71; H, 3.89; N, 18.93. Found: C, 41.60; H, 3.86; N, 19.01. Calcd for $Fe_2$(5,6-$Me_2$-HPTB)(OH)$(NO_3)_4 \cdot 2H_2O$, $C_{43}H_{54}Fe_2N_{14}O_{16}$: C, 45.52; H, 4.80; N, 17.28; Fe, 9.84. Found: C, 45.82; H, 4.98; N, 16.96; Fe, 9.22. Calcd for $Fe_2$(*N*-Et-HPTB)(OH)$(NO_3)_4 \cdot H_2O$, $C_{43}H_{52}Fe_2N_{14}O_{15}$: C, 46.28; H, 4.69; N, 17.56; Fe, 10.00. Found: C, 46.67; H, 4.89; N, 17.56; Fe, 9.64.

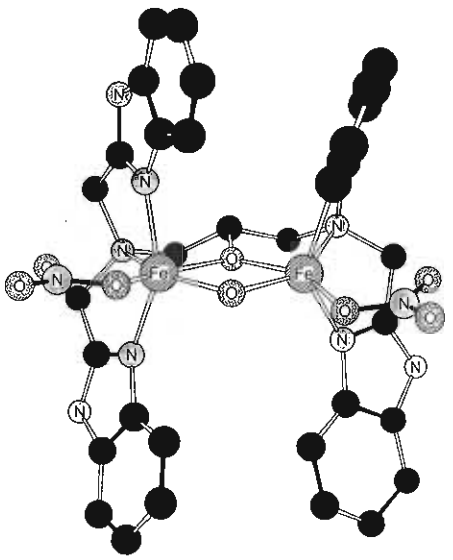

**Figure 2.** Representation of the $[Fe_2(HPTB)(OH)(NO_3)_2](NO_3)_2$ structure.

$^{57}$Fe-enriched samples of $[Fe_2(HPTB)(OH)(NO_3)_2](NO_3)_2$ were prepared by using 1 mg of 70% enriched $^{57}Fe_2O_3$ dissolved in 10 mL of hot concentrated $HNO_3$. The $HNO_3$ was evaporated, and the resultant solid was redissolved in methanol and then treated with 3.9 mg of HPTB (final volume 10 mL).

$^{18}$O-labeled hydrogen peroxide was prepared from $^{18}O_2$ (97% or 50% isotopic abundance, Isotec) by the published procedure.[35]

**Methods.** Conductivity measurements were obtained on a Yellow Springs conductivity bridge with a range of concentrations from 0.2 to 0.8 mM complex in acetonitrile. For the peroxide complex a small amount (1–2 $\mu$L) of 30% $H_2O_2$ was added to the same stock solution of precursor complex to compare the two measurements directly.

X-ray absorption spectra (XAS) were collected between 6.9 and 7.9 keV at beamline X-9A of the National Synchrotron Light Source (NSLS) at Brookhaven National Laboratories. The monochromator was calibrated by using the 7113.0-eV 1s → 3d peak in the XAS spectrum of $[Et_4N][FeCl_4]$ (suspended in DUCO Cement). The XAS data for the solid samples were obtained at ambient temperature in transmission mode with $A_{exp}$ ($-\log(C_f/C_0)$) determined from an incident ($C_0$) and final ($C_f$) ionization detector. The XAS data for the sample in frozen methanol solution were obtained at 100 K and $A_{exp}$ ($C_f/C_0$) was determined from an incident ($C_0$) ionization detector and a final Lytle fluorescence ($C_f$) detector with a Mn filter and Soller slits. As previously described, a modification of the program EXAPLT was employed to extract $\chi$ from $A_{exp}$ with a three-region cubic spline function.[36] Least-squares refinements to determine iron–ligand distances used the Newton–Gauss algorithm and were performed with locally developed software. The refinements reported were on $\chi k^3$, and the function minimized was $R = [\sum k^6(\chi_c - \chi)^2/n]^{1/2}$, where the sum is over $n$ data points between 2 and 13 Å$^{-1}$.

Magnetic susceptibility data were recorded over a temperature range of 10–300 K at a measuring field of 2.0 kOe with an SHE Corp. VTS-50 superconducting SQUID susceptometer interfaced with an IBM 9000 computer system. The temperature dependence data for $Fe_2$(*N*-Et-HPTB)(OH)$(NO_3)_4 \cdot 2H_2O$ and $Fe_2$(5,6-$Me_2$-HPTB)(OH)$(NO_3)_4 \cdot 3H_2O$ were analyzed by using the Heisenberg–Dirac–van Vleck spin Hamiltonian $\mathcal{H} = -2JS_1 \cdot S_2$. Details of the data collection and fitting are provided elsewhere.[33]

$^1$H NMR spectra were obtained on a Nicolet NT-300, an IBM AC-300, or a Varian Unity-300 NMR spectrometer. Temperature calibra-

(15) Norman, R. E.; Yan, S.; Que, L., Jr.; Backes, G.; Ling, J.; Sanders-Loehr, J.; Zhang, J. H.; O'Connor, C. J. *J. Am. Chem. Soc.* **1990**, *111*, 1554–1562.
(16) Vincent, J. B.; Huffman, J. C.; Christou; Li, Q.; Nanny, M. A.; Hendrickson, D. N.; Fong, R. H.; Fish, R. H. *J. Am. Chem. Soc.* **1988**, *110*, 6898–6900.
(17) Stenkamp, R. E.; Sieker, L. C.; Jensen, L. H. *J. Am. Chem. Soc.* **1984**, *106*, 618–622.
(18) Nordlund, P.; Sjöberg, B.-M.; Eklund, H. *Nature (London)* **1990**, *345*, 593–598.
(19) Niederhoffer, E. C.; Timmons, J. H.; Martell, A. E. *Chem. Rev.* **1984**, *84*, 137–203.
(20) Tyeklar, Z.; Ghosh, P.; Karlin, K. D.; Farooq, A.; Cohen, B. I.; Cruse, R. W.; Gultneh, Y.; Haka, M. S.; Jacobson, R. R.; Zubieta, J. *ACS Symp. Ser.* **1988**, *372*, 85–104.
(21) Tyeklar, Z.; Karlin, K. D. *Acc. Chem. Res.* **1989**, *22*, 241–248.
(22) Kitajima, N.; Fujisawa, K.; Moro-oka, Y.; Toriumi, K. *J. Am. Chem. Soc.* **1989**, *111*, 8975–8976.
(23) Jacobson, R. R.; Tyeklar, Z.; Farooq, A.; Karlin, K. D.; Liu, S.; Zubieta, J. *J. Am. Chem. Soc.* **1988**, *110*, 3690–3692.
(24) Abbreviations used: HPTB = *N,N,N',N'*-tetrakis(2-benzimidazolylmethyl)-2-hydroxy-1,3-diaminopropane; 5,6-$Me_2$-HPTB = 5,6-dimethylbenzimidazole derivative of HPTB; 5-Me-HXTA = *N,N'*-(2-hydroxy-5-methyl-1,3-xylylene)bis(*N*-(carboxymethyl)glycine); DBE = 2-[bis(2-benzimidazolylmethyl)amino]ethanol; N3 = bis(2-benzimidazolylmethyl)amine; TTP = *meso*-tetra-*p*-tolylporphyrin; OEP = octaethylporphyrin; $HB(pz)_3$ = hydrotris(pyrazolyl)borate; OBz = benzoate; pyN5 = 3,6,10,13,19-pentaazabicyclo[13.3.1]nonadeca-1-(19),15,17-triene.
(25) Kimura, E.; Kodama, M.; Machida, R.; Ishizu, K. *Inorg. Chem.* **1982**, *21*, 595–602.
(26) Kitajima, N.; Hideno, F.; Moro-oka, Y.; Mizutani, Y.; Kitagawa, T. *J. Am. Chem. Soc.* **1990**, *112*, 6402–6403.
(27) Ménage, S.; Brennan, B. A.; Juarez-Garcia, C.; Münck, E.; Que, L., Jr. *J. Am. Chem. Soc.* **1990**, *112*, 6423–6425.
(28) Sawyer, D. T.; McDowell, M. S.; Spencer, L.; Tsang, P. K. S. *Inorg. Chem.* **1989**, *28*, 1166–1170.
(29) (a) Nishida, Y.; Takeuchi, M.; Shimo, H.; Kida, S. *Inorg. Chim. Acta* **1984**, *96*, 115–119. (b) Nishida, Y.; Takeuchi, M. *Z. Naturforsch.* **1987**, *42B*, 52–54.
(30) (a) Murch, B. P.; Bradley, F. C.; Que, L., Jr. *J. Am. Chem. Soc.* **1986**, *108*, 5027–5028. (b) Murch, B. P. Ph.D. Thesis, Cornell University, 1987.
(31) Micklitz, W.; Bott, S. G.; Bentson, J. G.; Lippard, S. J. *J. Am. Chem. Soc.* **1989**, *111*, 372–374.
(32) McKee, V.; Zvagulis, M.; Dagdigian, J. V.; Patch, M. G.; Reed, C. A. *J. Am. Chem. Soc.* **1984**, *106*, 4765–4772.
(33) Chen, Q.; Lynch, J. B.; Gomez-Romero, P.; Ben-Hussein, A.; Jameson, G. B.; O'Connor, C. J.; Que, L., Jr. *Inorg. Chem.* **1988**, *27*, 2673–2681.
(34) This method differs from the published procedure in ref 29a in that the $Et_3N$ is eliminated. The base is unnecessary and a crystalline product is formed more readily without the base.
(35) Sitter, A. J.; Terner, J. *J. Labelled Comp. Radiopharm.* **1984**, *22*, 461–465.
(36) Scarrow, R. C.; Maroney, M. J.; Palmer, S. M.; Que, L., Jr.; Roe, A. L.; Salowe, S. P.; Stubbe, J. *J. Am. Chem. Soc.* **1987**, *109*, 7857–7864.

**Table I.** Comparison of Metric Parameters of $[Fe_2(5,6\text{-}Me_2\text{-}HPTB)(OH)(NO_3)_2](NO_3)_2$ and $[Fe_2(DBE)_2(OBz)_2](ClO_3)_2$

| EXAFS data fits of 10 mM $[Fe_2(5,6\text{-}Me_2\text{-}HPTB)(OH)(NO_3)_2](NO_3)_2$ in MeOH[a,b] | | | | | | | | selected bond lengths of $[Fe_2(DBE)_2(OBz)_2](ClO_4)_2$[c] | |
|---|---|---|---|---|---|---|---|---|---|
| first-shell fit | | | | multishell fit | | | | | |
| $n$ | atom | $R$, Å | $\sigma^2$ | $n$ | atom | $R$, Å | $\sigma^2$ | bond | length, Å |
| 5 | N/O | 2.01 | 0.0044 | 5 | N/O | 2.01 | 0.0042 | Fe–O1 | 1.96 (1) |
| 1 | N/O | 2.41 | 0.0005 | 1 | N/O | 2.41 | 0.0005 | Fe–O1C | 1.99 (1) |
| | $F$ = 0.104[d] | | | 3.7 | C | 2.97 | 0.006 | Fe–O1′ | 2.03 (1) |
| | | | | 1 | Fe | 3.18 | 0.002 | Fe–N1B | 2.07 (2) |
| | | | | 4.6 | C | 4.25 | 0.006 | Fe–N1A | 2.09 (2) |
| | | | | | $F$ = 0.156[d] | | | Fe–N1 | 2.35 (2) |
| | | | | | | | | Fe–Fe | 3.21 (1) |

[a] This work. [b] Both solid and solution EXAFS data gave fits consistent with similar structures. [c] Reference 43. [d] $F$, goodness of fit, is defined as rms(dev)/rms(dat) where the function minimized is $R = [\sum k^6(\chi_c - \chi)/n]^{1/2}$.

tion for variable-temperature $^1H$ NMR experiments was accomplished with methanol/HCl solutions.[37] The value for the antiferromagnetic coupling, $J$, was evaluated from the temperature dependence of the isotropic shifts as previously described.[38] The concentrations of EtOH and acetone were determined by the method of standard addition using benzene as an internal integration standard.

UV–vis spectra were recorded on an HP 8451A diode array spectrometer. Resonance Raman spectra were obtained on a Spex 1403 spectrometer interfaced with a Spex Datamate using Spectra-Physics Models 2030 argon ion and 375B dye (Rhodamine 6G) lasers. Spectra were obtained at 79 K with use of a gold-plated copper cold finger in thermal contact with a dewar containing liquid nitrogen.[39] Raman frequencies are referenced against an external $Na_2SO_4$ standard in frozen aqueous solution ($A_1$ stretch at 993 $cm^{-1}$).[40]

## Results and Discussion

**Structure and Properties of the "$Fe^{III}_2$(HPTB)" Precursor Complex.** Nishida and co-workers first formulated the complex of Fe(III) and HPTB as $Fe_2(HPTB)(NO_3)_5 \cdot 2EtOH$ on the basis of its elemental analysis.[29] Conductivity measurements indicated a 2:1 electrolyte and led to the suggestion of a ($\mu$-alkoxo)($\mu$-nitrato)diiron core for the complex with two terminal nitrates, i.e. $[Fe_2(HPTB)(\mu\text{-}NO_3)(NO_3)_2](NO_3)_2 \cdot 2EtOH$.[29] However, upon reexamination in our laboratory, several lines of evidence suggested that this formulation was incorrect and have led us to reformulate this compound as solvates of $[Fe_2(HPTB)(\mu\text{-}OH)(NO_3)_2](NO_3)_2$.

While the elemental analysis that we obtained of the HPTB complex was consistent with Nishida's formulation,[29a] it could also be made consistent with the alternative formulation by suitable manipulation of both the number and type of solvate molecules. $^1H$ NMR spectroscopy was used to clarify the solvate question; the amount of ethanol found in the parent complex varied from 0.2 to 0.8 molecule/complex depending on the extent of vacuum-drying, and in none of the samples did the ethanol:complex ratio approach 2:1. Furthermore, corresponding complexes of the *N*-ethyl and 5,6-dimethyl derivatives of HPTB afforded analyses more easily reconciled with the $\mu$-hydroxo formulation.

Efforts to clarify this problem with X-ray diffraction yielded a structure whose resolution was limited by the disorder in the solvent structure and by facile loss of solvent from the crystals.[41] Nevertheless, the spatial relationships of the various ligating atoms can be determined from the structure as represented in Figure 2. It features a ($\mu$-alkoxo)($\mu$-hydroxo)diiron core, with each iron being six-coordinate. The tertiary amine nitrogens of the HPTB ligand are trans to the hydroxo bridge, while terminal monodentate nitrates coordinate trans to the alkoxo bridge. The benzimidazoles are coordinated trans to each other and perpendicular to the approximate $Fe_2O_2$ plane. There appear to be $\pi$-stacking interactions between benzimidazoles on the two sides of the molecule, and such interactions may aid in stabilizing this structure. Similar ligand arrangements have been observed in the related complexes $[Fe_2(DBE)_2(NO_3)_2](NO_3)_2$[42] and $[Fe_2(DBE)_2(OBz)_2](ClO_4)_2$,[43] where DBE represents the mononucleating analogue of HPTB.

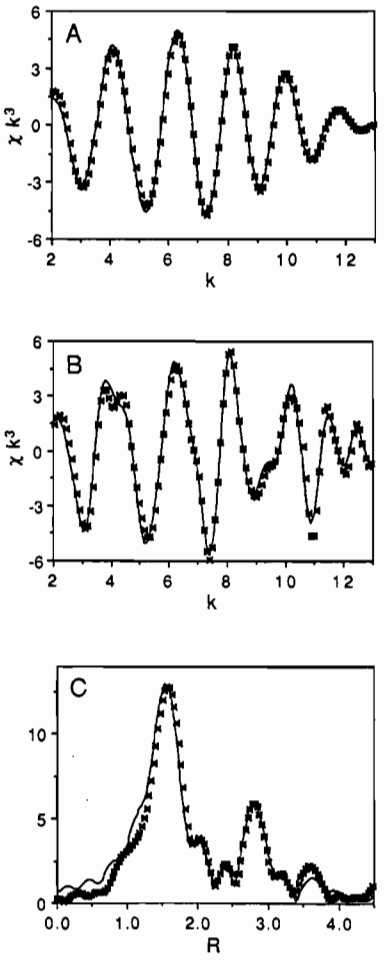


**Figure 3.** EXAFS data (*) and simulations (—) of $Fe_2(5,6\text{-}Me_2\text{-}HPTB)(OH)(NO_3)_4 \cdot 2H_2O$ in MeOH: (A) first-shell Fourier filtered (back-transformed 1.0–2.3 Å) $\chi k^3$ data; (B) multishell Fourier filtered (back-transformed 1.0–6.0 Å) $\chi k^3$ data; (C) Fourier transform of $\chi k^3$ data and simulation presented in panel B. Parameters for fits are as listed in Table I.

(37) Van Geet, A. L. *Anal. Chem.* **1970**, *6*, 679–680.
(38) (a) Maroney, M. J.; Kurtz, D. M., Jr.; Nocek, J. M.; Pearce, L. L.; Que, L., Jr. *J. Am. Chem. Soc.* **1986**, *108*, 6871–6879. (b) Que, L., Jr.; Maroney, M. J. *Met. Ions Biol. Syst.* **1987**, *21*, 87–120.
(39) Czernuszewicz, R. C.; Johnson, M. K. *Appl. Spectrosc.* **1983**, *37*, 297–298.
(40) The $A_1$ stretching frequency is at 983 $cm^{-1}$ for room-temperature aqueous solution; however, this resonance shifts to 993 $cm^{-1}$ in frozen solution.
(41) $Fe_2(HPTB)(OH)(NO_3)_4 \cdot 1.5H_2O \cdot 0.5EtOH$ crystallizes in the space group $P\bar{1}$ with cell constants $a$ = 15.532 (7) Å, $b$ = 16.854 (6) Å, $c$ = 12.504 (6) Å, $\alpha$ = 108.78 (3)°, $\beta$ = 103.92 (4)°, and $\gamma$ = 62.88 (3)°. The data was collected to a peak width of 2°. The structure was solved by using isotropic temperature factors and refined to $R$ = 0.17; the crystal decomposed before $\psi$ scans could be made. Several other crystals of the same compound gave similar low-resolution data.
(42) Nishida, Y.; Shimo, H.; Takahashi, K.; Kida, S. *Mem. Fac. Sci. Kyushu Univ., Ser. C* **1984**, *14*, 301–306.
(43) Ménage, S.; Que, L., Jr. *Inorg. Chem.* **1990**, *29*, 4293–4297.

**Table II.** $^1$H NMR Assignments and Comparison (ppm)[a]

| | A | A + $H_2O_2$ | B | B + $H_2O_2$ | C | C + $H_2O_2$ | D | E | F |
|---|---|---|---|---|---|---|---|---|---|
| $J$, $cm^{-1}$ | ~−20[b] | ~−70[b] | −24.6[c] | | −22.1[c] | | ~−100[b] | −20[c] | −117 |
| methylene? | | 67 (br) | | 71 | | 63 | | | |
| methylene? | | 36 (br) | | 35 | | 37 | | | |
| NH | 48 | 28 | 47 | 29 | | | 15.9 | 47.9 | 17 |
| NH | 44 | 26 | 42 | 27 | | | 13.8 | | |
| | 43[d] | 26[d] | | | 26 | 40 | | | |
| C7 | 35 | 17 | 35 | 17 | 34 | 17 | 12.3 | 36 | 11.7[e] |
| C7 | | | | | | | 9.5 | | |
| | 12 | 10, 7 | | 8.8, 7.4 | | | | | 6.8 (br) |
| C5 or C6 | | 5.8 | | | | | | | 6.7 |
| C5 or C6 | | 5.3 | | | | | 6.9 | | |
| C5 or C6 | | | | | | | 6.1 | | |
| methyl | | | 9.04 | 3.9, 4.1 | | | | | |
| *N*-ethyl | | | | | 7.9, 11.1 | 5.5, 6.0, 6.7 | | | |
| OBz | | | | | | | | 10.6 | n.r.[f] |
| ref | this work | | this work | | this work | | 33 | 43 | 14 |

[a] A = $Fe_2$(HPTB)(OH)$(NO_3)_4$; B = $Fe_2$(5,6-$Me_2$-HPTB)(OH)$(NO_3)_4$; C = $Fe_2$(*N*-Et-HPTB)(OH)$(NO_3)_4$; D = $[Fe_4(HPTB)_2(O)_2(O_2CC_6D_5)_2](ClO_4)_2(OTs)_2$; E = $Fe_2(DBE)_2(OBz)_2(ClO_4)_2$; F = $Fe_2O(N3)_2(OBz)_2(ClO_4)_2$. [b] Determined by variable-temperature $^1$H NMR spectroscopy. [c] Determined by variable-temperature susceptibility measurements using a SQUID susceptometer. [d] Seen with both $D_2O$ exchange of the NH protons and the *N*-ethyl derivative. [e] Only the 17 ppm resonance was assigned in the paper; however, the resonances at 11.7, 6.8, and 6.7 ppm were assigned as originating from the ligand, bis(2-benzimidazolylmethyl)amine (N3). The assignments are by analogy to the other complexes. [f] Not reported.

An EXAFS analysis of the parent complex, as a solid and in methanolic solution, was carried out to confirm the crystal structure and obtain metric details of the metal coordination environment. Figure 3 shows first-shell and multishell fits to the methanolic solution data which consist of 5 O/N at 2.01 Å, 1 O/N at 2.41 Å, 3.7 C at 2.97 Å, and 1 Fe at 3.18 Å.[44] These structural parameters are consistent with the proposed structure and match well with the structural parameters obtained crystallographically for the related DBE complex (Table I). The 2.01-Å average bond length is consistent with Fe–O bonds found for various complexes with $Fe_2(\mu\text{-OR})_2$ cores ($r_{av}$ = 2.02 Å)[42,43,45-48] and Fe–N bonds of benzimidazole ligands ($r_{av}$ = 2.07 Å).[14,33,43,49,50] The 2.41-Å distance is typical of Fe–amine bonds which are usually elongated in tripodal ligands that form five-membered chelate rings; this elongation appears even more pronounced for tripodal ligands with pendant benzimidazoles, as illustrated by $[Fe_2(DBE)_2(OBz)_2](ClO_4)_2$ (2.35 Å)[43] and $[Fe_2O(OBz)_2(N3)_2](ClO_4)_2$ (2.38 Å).[14] The 3.18-Å Fe–Fe separation is typical of complexes with $Fe_2O_2$ cores.[42,43,45-48] The EXAFS data thus appear to corroborate the low-resolution crystal structure.

The magnetic properties of the *N*-Et-HPTB and 5,6-$Me_2$-HPTB complexes were evaluated by variable-temperature magnetic susceptibility measurements on a SQUID susceptometer. Excellent fits of the data were obtained, and that for the 5,6-$Me_2$-HPTB complex is shown in Figure 4; the *N*-Et and 5,6-$Me_2$ complexes exhibit $J$ values of −22.1 and −24.6 $cm^{-1}$, respectively. These values are typical of bis($\mu$-alkoxo)diiron(III) complexes but would also be expected for complexes with ($\mu$-alkoxo)($\mu$-hydroxo)diiron(III) cores.[47,48]

The $^1$H NMR spectrum of $[Fe_2$(5,6-$Me_2$-HPTB)(OH)$(NO_3)_2](NO_3)_2$ in $CD_3CN$/DMSO-$d_6$ exhibits features at 42 and 47 ppm, which disappear upon addition of $D_2O$ or $CD_3OD$ (Figure 5, Table II). These features are also absent in the spectrum of the *N*-Et derivative and thus associated with the benzimidazole N–H protons. The feature at 35 ppm is found in all three HPTB complexes and associated with the C7-H protons by analogy to previous studies of HPTB complexes.[33] The C7–H isotropic shift

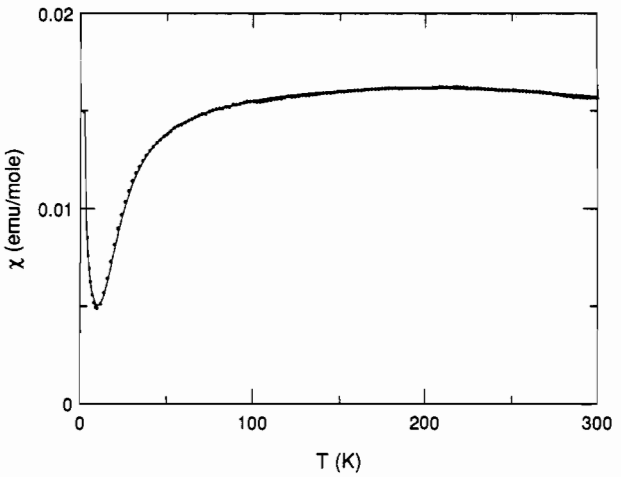


**Figure 4.** Variable-temperature magnetic susceptibility data: fit of SQUID magnetic susceptibility data of $Fe_2$(5,6-$Me_2$-HPTB)(OH)$(NO_3)_4 \cdot 2H_2O$ (the EXAFS sample) ($J$ = −24.6 $cm^{-1}$, $g$ = 2.00, TIP = 0.004 97 cgsu, 0.38% mononuclear high-spin ferric impurity).

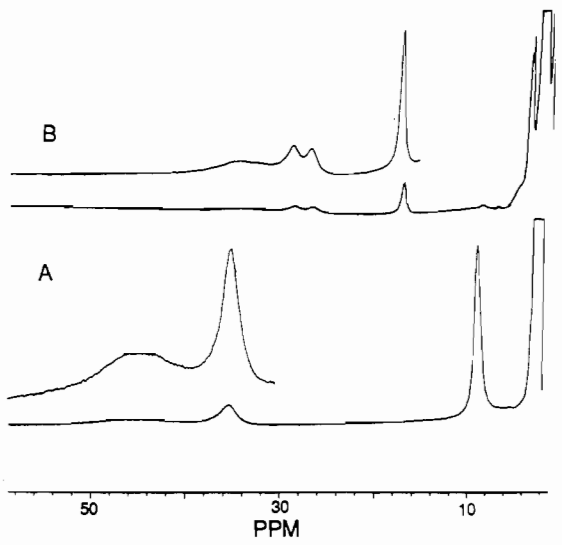


**Figure 5.** $^1$H NMR spectra: (A) 3 mM $[Fe_2$(5,6-$Me_2$-HPTB)(OH)$(NO_3)_2](NO_3)_2$ in $CD_3CN$/20% DMSO-$d_6$; (B) same solution as in (A) with 2 equiv of $H_2O_2$ added.

(44) Since both the solid $Fe_2$(*N*-Et-HPTB)(OH)$(NO_3)_4$ and the methanolic solution of $Fe_2$(5,6-$Me_2$HPTB)(OH)$(NO_3)_4$ yielded similar parameters, we report only one set of values for clarity.

(45) Snyder, B. S.; Patterson, G. S.; Abrahamson, A. J.; Holm, R. H. *J. Am. Chem. Soc.* **1989**, *111*, 5214–5223.
(46) Bertrand, J. A.; Eller, P. G. *Inorg. Chem.* **1974**, *13*, 927–934.
(47) Chiari, B.; Piovesana, A. O.; Tarantelli, T.; Zanazzi, P. F. *Inorg. Chem.* **1984**, *23*, 3398–3404.
(48) Ou, C. C.; Lalancette, R. A.; Potenza, J. A.; Schugar, H. J. *J. Am. Chem. Soc.* **1978**, *100*, 2053–2057.
(49) Gómez-Romero, P.; Witten, E. H.; Reiff, W. M.; Backes, G.; Sanders-Loehr, J.; Jameson, G. B. *J. Am. Chem. Soc.* **1989**, *111*, 9039–9047.
(50) Gomez-Romero, P.; Witten, E. H.; Reiff, W. M.; Jameson, G. B. *Inorg. Chem.* **1990**, *29*, 5211–5217.

**Table III.** Electronic and Vibrational Properties of Iron Peroxo Complexes[a]

| | $\lambda_{max}$ ($\epsilon$) | $\nu$(Fe–O) ($^{18}$O) | $\nu$(O–O) ($^{18}$O) | bonding mode | ref |
|---|---|---|---|---|---|
| oxyhemerythrin | 500 (2300) | 503 (480) | 844 (797) | $\eta^1$ | 55 |
| Hr($^{16}$O$^{18}$O) | | 501, 485 | 825, 818 | | |
| $[Fe_2(HPTB)(O_2)(NO_3)_2]^+$ ($H_2O$) | 560 (2200) | 476 (457) | 895 (854) | $\mu$-$\eta^1$:$\eta^1$ | this work |
| $[Fe_2(HPTB)(O_2)(NO_3)_2]^+$ (MeOH) | 604 (1600) | 470 | 890 | $\mu$-$\eta^1$:$\eta^1$ | this work |
| $[Fe_2(5,6\text{-}Me_2\text{-}HPTB)(O_2)(NO_3)_2]^+$ (MeOH) | 600 (1500) | 474 | 888 | $\mu$-$\eta^1$:$\eta^1$ | this work |
| $[Fe_2(N\text{-Et-HPTB})(O_2)(NO_3)_2]^+$ (MeOH) | 606 (1500) | 476 (460) | 890 (838) | $\mu$-$\eta^1$:$\eta^1$ | this work |
| $[Fe_2(N\text{-Et-HPTB})(O_2)(OBz)]^{2+}$ | 588 (1500) | 476 | 900 | $\mu$-$\eta^1$:$\eta^1$ (?) | 27 |
| $[Fe(HB(3,5\text{-}i\text{-}Pr_2pz)_3](OBz)]_2O_2$ | 679 | 418 (409) | 876 (827) | $\mu$-$\eta^1$:$\eta^1$ (?) | 26 |
| $[Fe_2(5\text{-Me-HXTA})(O_2)(OAc)]^{2-}$ | 480 (2370) | n.o. | 884 | $\mu$-$\eta^1$:$\eta^1$ | 30 |
| $\{[Fe(pyN5)]_2O_2\}^{4+}$ | 540 (190) | n.r. | n.r. | $\mu$-$\eta^1$:$\eta^1$ (?) | 25 |
| $\{[Fe(Ph_3PO)_4]_2O_2\}^{4+}$ | 576 (3540) | n.o. | 882 (848) | $\mu$-$\eta^1$:$\eta^1$ (?) | 28 |
| $\{[Fe(TMP)]_2O_2\}$ | n.r. | 574 (547) | n.o. | $\mu$-$\eta^1$:$\eta^1$ (?) | 56 |
| $Fe(OEP)O_2$[b] | | n.o. | 806 (759) | $\eta^2$ | 58 |
| $[Fe^{III}(EDTAH)O_2]^{2-}$ | 520 (530) | n.o. | 815 | $\eta^2$ | 57 |
| $[Fe^{III}(EDTAH)(^{16}O^{18}O)]^{2-}$ | | n.o. | 794 | | |
| $[Fe_6(O)_2(O_2)(OBz)_{12}(OH_2)]$ | 534 (1590) | n.r. | 853 | $\mu_4$ | 31 |

[a] Units: $\lambda_{max}$, nm; $\epsilon$, $M^{-1}$ $cm^{-1}$); vibrational data, $cm^{-1}$. n.o. = not observed; n.r. = not reported. [b] Infrared data.

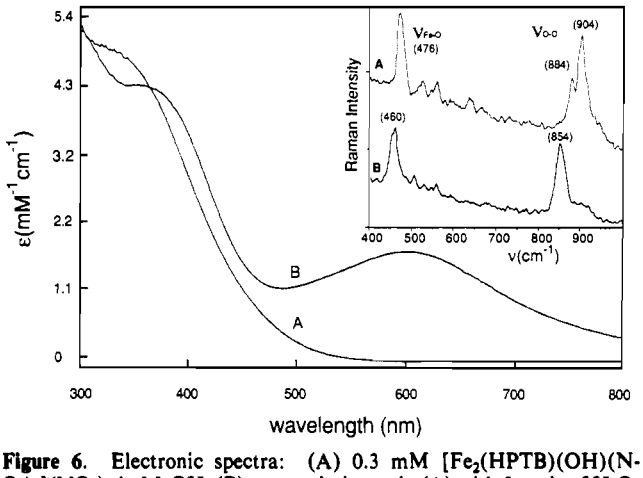


**Figure 6.** Electronic spectra: (A) 0.3 mM $[Fe_2(HPTB)(OH)(NO_3)_2](NO_3)_2$ in MeOH; (B) same solution as in (A) with 5 equiv of $H_2O_2$ added. Inset: (A) resonance Raman spectrum of 3 mM $[Fe_2(HPTB)(OH)(NO_3)_2](NO_3)_2$ with 5 mM $H_2O_2$ in $H_2O$ at 79 K obtained by using 575 nm and averaging five 5-s scans with 80-mW power at the sample; (B) resonance Raman spectrum of 3 mM $[Fe_2(HPTB)(OH)(NO_3)_2](NO_3)_2$ with 5 mM $H_2{}^{18}O_2$ in $H_2O$ at 79 K obtained by using 575 nm and averaging five 5-s scans with 80-mW power at the sample.

shows a temperature dependence in the range −60 to +30 °C that corresponds to a $J$ value of −20 (3) $cm^{-1}$, in agreement with the solid susceptibility measurements, suggesting that the ($\mu$-alkoxo)($\mu$-hydroxo)diiron(III) core is retained in solution. Other features of the $^1$H NMR spectrum are indistinctive and will not be discussed further.

**$[Fe_2(HPTB)(OH)(NO_3)_2](NO_3)_2$ + $H_2O_2$.** The electronic spectrum of $[Fe_2(HPTB)(OH)(NO_3)_2](NO_3)_2$ in MeOH exhibits a $\lambda_{max}$ at 340 nm ($\epsilon$ = 7300 $M^{-1}$ $cm^{-1}$),[51] which arises from a benzimidazole-to-iron charge-transfer transition (Figure 6). When hydrogen peroxide is added, the color changes from orange to blue-green and a new feature appears near 600 nm. This band, observable in a variety of solvents including water, methanol, acetone, acetonitrile, DMF, and DMSO, shows some solvent dependence; for example, $\lambda_{max}$ = 560 nm ($\epsilon$ = 2200 $M^{-1}$ $cm^{-1}$) in $H_2O$ and $\lambda_{max}$ = 604 nm ($\epsilon$ = 1600 $M^{-1}$ $cm^{-1}$) in MeOH (Figure 6, Table III). The HPTB complex has a very high affinity for peroxide; by the use of Job's method of continuous variations, the $[Fe_2(HPTB)(OH)(NO_3)_2](NO_3)_2$ to $H_2O_2$ binding stoichiometry is demonstrated to be 1:1, and $K'_{eff}$ is estimated to be greater than $10^6$ $M^{-1}$ in MeOH. Application of a vacuum does not result in loss of the blue-green color, which indicates that the peroxide binding is irreversible. Under the appropriate conditions, the peroxide complex is stable enough to allow spectroscopic characterization of the peroxide binding mode. In fact, its electronic and $^1$H NMR spectra may be observed at ambient temperature; however, low-temperature techniques were required to observe the resonance Raman spectra due to facilitated decomposition of the complex by laser irradiation.

The resonance Raman spectrum of the peroxide adduct shows the new spectral feature at ca. 600 nm to be a peroxide-to-iron charge-transfer transition. With 575-nm excitation at 79 K, two features are observed; one is assigned to $\nu$(Fe–O) at 476 $cm^{-1}$, and the other, which appears as a Fermi doublet centered at 895 $cm^{-1}$, is assigned to $\nu$(O–O) (Figure 6 inset, Table III).[52,53] Accordingly, the observed vibrations shift to 457 and 854 $cm^{-1}$, respectively, with the use of $H_2{}^{18}O_2$; these are in good agreement with the calculated shifts predicted by using a simple diatomic model, $\nu$(Fe–$^{18}$O) = 455 $cm^{-1}$ and $\nu$($^{18}$O–$^{18}$O) = 854 $cm^{-1}$. The $\nu$(O–O) Fermi doublet also collapses into a single peak upon $^{18}$O substitution. The use of 488- and 621-nm excitation affords Raman features that are less enhanced than those obtained with 575-nm excitation, thereby corroborating the charge-transfer assignment for the 600-nm band. The peroxide adduct of the corresponding $N$-ethyl derivative exhibits similar Raman features (Table III).

The spectra are unaffected by the presence of $D_2O$, suggesting that neither peroxide oxygen is protonated. In contrast, the Raman features of oxyhemerythrin, which has an $\eta^1$-hydroperoxide moiety, are affected by $D_2O$ ($\Delta\nu$(Fe–O) = −3 $cm^{-1}$ and $\Delta\nu$(O–O) = +4 $cm^{-1}$).[8] Since peroxide bound in $\eta^1$ and $\mu$-$\eta^1$ modes would be sufficiently basic to be readily protonated in aqueous solution, the absence of a shift in the Raman vibrations in $D_2O$ strongly suggests that both peroxide oxygens are coordinated to a metal center. Unfortunately, efforts to determine the symmetry of peroxide binding by the use of statistically mixed labeled $H_2O_2$ (50% $^{18}$O) to form the peroxide complex were uninformative due to a lack of resolution in the isotopically shifted peaks.

The vibrational energies of the $[Fe_2(HPTB)(OH)(NO_3)_2](NO_3)_2$/peroxide complex are in the same range as other (di)ferric peroxide complexes (Table III). The $\nu$(Fe–O) value of 476 $cm^{-1}$ is close to that found for oxyHr;[8,54,55] however, not all the reported ferric peroxide complexes exhibit this vibration.[30,57,58] The $\nu$(O–O)

(51) The complexes formed with the derivatized ligands also have a similar feature. $Fe_2(5,6\text{-}Me_2\text{-HPTB})(OH)(NO_3)_4$ has a $\lambda_{max}$ at 350 $cm^{-1}$ ($\epsilon$ = 7500 $M^{-1}$ $cm^{-1}$), and $Fe_2(N\text{-Et-HPTB})(OH)(NO_3)_4$ has a $\lambda_{max}$ at 340 $cm^{-1}$ ($\epsilon$ = 6000 $M^{-1}$ $cm^{-1}$).

(52) Since the complex was not very soluble when $SO_4^{2-}$ or other internal standards were added, aqueous 0.5 M $Na_2SO_4$ was loaded on an adjacent port and used as an external reference before and after the experiment.

(53) Nishida and co-workers have also reported the resonance Raman spectrum of this peroxide complex with $\nu$(Fe–O) at 495 $cm^{-1}$ and $\nu$(O–O) at 890 $cm^{-1}$. However, the solvent system was not noted and these bands are sensitive to solvent (Table III).[29b]

(54) Dunn, J. B. R.; Shriver, D. F.; Klotz, I. M. *Proc. Natl. Acad. Sci. U.S.A.* **1973**, *70*, 2582–2584.

(55) Kurtz, D. M.; Shriver, D. F.; Klotz, I. M. *J. Am. Chem. Soc.* **1976**, *98*, 5033–5035.

(56) Wagner, W.-D.; Paeng, I. R.; Nakamoto, K. *J. Am. Chem. Soc.* **1988**, *110*, 5565–5567.

**Table IV.** Mössbauer Parameters

| | $\delta$, mm/s | $\Delta E_Q$, mm/s | intens, % | ref |
|---|---|---|---|---|
| $[Fe(HBpz_3)(OAc)]_2O$ | 0.52 | 1.60 | 100 | 60 |
| methemerythrin | 0.46 | 1.57 | 100 | 59 |
| oxyhemerythrin | 0.52 | 1.92 | 50 | 59 |
| | 0.48 | 1.00 | 50 | |
| $Fe_2(HPTB)(OH)(NO_3)_4$ | 0.49 | 0.66 | 100 | this work |
| $Fe_2(HPTB)(OH)(NO_3)_4 + H_2O_2$ | 0.54 | 0.84 | 100 | this work |
| $[Fe_2(N\text{-Et-HPTB})(OBz)]^{2+} + O_2$ | 0.52 | 0.72 | 100 | 27 |
| $[Fe_2(5\text{-Me-HXTA})(O_2)(OAc)]^{2-}$ | 0.54 | 1.04 | 100 | 30b |

features for these complexes also exhibit a range of values (815–904 $cm^{-1}$), with the $\eta^2$ complexes having values near 800 $cm^{-1}$ and those with postulated $\mu$-$\eta^1$:$\eta^1$ coordination having values near 900 $cm^{-1}$. Interestingly, the sole $\eta^1$ complex (oxyhemerythrin) and the $\mu_4$ complex exhibit intermediate values near 844 $cm^{-1}$. The rationale for these observations is still unclear.

The Mössbauer spectrum of $^{57}$Fe-enriched 1.2 mM $[Fe_2(HPTB)(OH)(NO_3)_2](NO_3)_2$ in methanol exhibits a broad quadrupole doublet with parameters typical of high-spin ferric centers, $\delta$ = 0.49 mm/s and $\Delta E_Q$ = 0.66 mm/s. The absence of magnetic hyperfine structure at 4.2 K is consistent with the coupled diferric structure discussed earlier. Addition of $H_2O_2$ affords a new quadrupole doublet with $\delta$ = 0.54 mm/s and $\Delta E_Q$ = 0.84 mm/s. That the parameters of both iron centers are similarly affected by peroxide binding suggests that the peroxide binds to both of the ferric irons in a symmetric arrangement (Table IV).

Peroxide binding effects a dramatic change in the $^1$H NMR spectrum of $[Fe_2(5,6\text{-}Me_2\text{-}HPTB)(OH)(NO_3)_2](NO_3)_2$; the proton resonances become sharper and less paramagnetically shifted (Figure 5, Table II). Similar peak patterns are observed for the HPTB complex in a variety of solvents ($CD_3CN$/DMSO-$d_6$, $CD_3OD$, or $D_2O$). A $^1$H NMR titration study of $[Fe_2(HPTB)(OH)(NO_3)_2](NO_3)_2$ with $H_2O_2$ shows that the peroxide species is completely formed when 1 equiv of $H_2O_2$ is added/metal complex and both sets of resonances from the complexed and uncomplexed species are observable when less than 1 equiv of $H_2O_2$ is added/metal complex. Thus binding is at the slow-exchange limit and no intermediate species is observed.

For the $[Fe_2(HPTB)(OH)(NO_3)_2](NO_3)_2/H_2O_2$ adduct, the N–H resonances shift from 48 and 44 ppm to 28 and 26 ppm, respectively, while the C7 resonance shifts from 35 ppm to 17 ppm, indicating a significant increase in the antiferromagnetic coupling between the ferric centers upon peroxide binding. The temperature dependence of the resonances of the peroxide complex shows a slight positive slope with increasing temperature, suggesting that the Néel point shifts to above room temperature[38b] in the peroxide complex. A precise value for the coupling constant, $-J$, is difficult to deduce when $-J$ becomes large because of the insensitivity of isotropic shift to temperature changes.[38b] However, comparisons of the isotropic shifts with those of other diferric complexes with the bis(2-benzimidazolylmethyl)amine structural unit indicate that $-J$ is smaller than the 100–120-$cm^{-1}$ value associated with ($\mu$-oxo)diiron complexes but larger than the 20-$cm^{-1}$ value associated with bis($\mu$-alkoxo)diiron complexes (Table II). The C7 benzimidazole protons of the oxo-bridged complex $[Fe_2O(OBz)_2(N3)_2](ClO_4)_2$ ($-J$ = 117 $cm^{-1}$) resonate at 11.7 ppm, while those of the dialkoxo-bridged complex $[Fe_2(DBE)_2(OBz)_2](ClO_4)_2$ ($-J$ = 20 $cm^{-1}$) resonate at 36 ppm.[43] Since the isotropic shift is proportional to the magnetic susceptibility of the complex on the assumption that the hyperfine splitting value remains constant,[38] the observed shift to 17 ppm for the C7 proton of the peroxide complex corresponds to a $\chi$ that is ca. 15% of the value for the uncoupled case or a $-J$ of 70 (10) $cm^{-1}$.

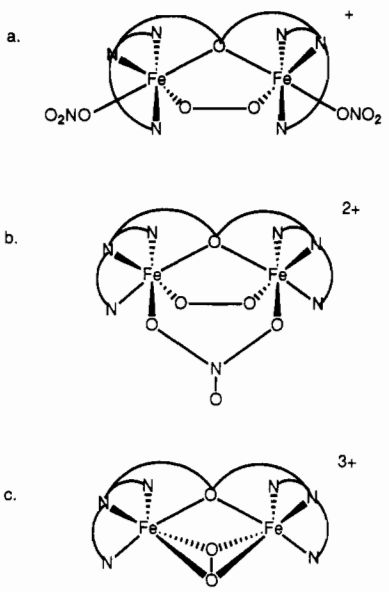


**Figure 7.** Possible structures for the $[Fe_2(HPTB)(OH)(NO_3)_2](NO_3)_2/H_2O_2$ complex compatible with the spectroscopic data.

The increase in antiferromagnetic coupling between the ferric centers indicates that a new coupling pathway is generated upon peroxide binding. A $\mu$-$\eta^1$-peroxide can be eliminated as a plausible mode of peroxide binding, since such a structure would be expected to exhibit a $J$ value comparable to those of complexes with $Fe_2O_2$ cores ($-J$ = 5–20 $cm^{-1}$). Given the above observations, the two modes of peroxide binding that remain as possibilities are $\mu$-$\eta^1$:$\eta^1$ and $\mu$-$\eta^2$:$\eta^2$ modes (Figure 7). Such binding modes are exemplified by two copper complexes, both of which are structurally characterized, i.e. $\{[Cu(TPA)]_2(trans\text{-}\mu\text{-}\eta^1\text{:}\eta^1\text{-}O_2)\}X_2$[23] and $[Cu\{HB(3,5\text{-}i\text{-}Pr_2pz)_3\}]_2(\mu\text{-}\eta^2\text{:}\eta^2\text{-}O_2)$.[22] Both binding modes can mediate strong antiferromagnetic coupling, at least for dicopper complexes. In iron chemistry, the $\mu$-$\eta^1$:$\eta^1$ mode is exemplified by the complex $[Fe(TPP)]_2O_2$.[61] $^1$H NMR spectra of this metastable intermediate at low temperature show that the pyrrole shifts are only slightly larger than those of the $\mu$-oxo species $[Fe(TPP)]_2O$, suggesting a $J$ value approximately $-100$ $cm^{-1}$ for the $\mu$-$\eta^1$:$\eta^1$-peroxo complex. For the HPTB complex, the peroxide is likely to be bound in a cis $\mu$-$\eta^1$:$\eta^1$ mode, because of the presence of the $\mu$-alkoxo group. Such a binding mode has been structurally characterized in a dicobalt complex, $[Co_2(bpmp)(OBz)O_2](BF_4)_2$, with a $\mu$-phenoxo, a $\mu$-$\eta^1$:$\eta^1$-peroxo, and a $\mu$-benzoato bridge.[62]

Although none of the spectroscopic methods applied can be used alone to deduce the solution structure of the $[Fe_2(HPTB)(OH)(NO_3)_2](NO_3)_2$/peroxide complex, a consistent picture emerges when the data are taken together. The Job plot and the $^1$H NMR titration data indicate a 1:1 $[Fe_2(HPTB)(OH)(NO_3)_2](NO_3)_2$:$H_2O_2$ binding stoichiometry. The Raman, Mössbauer, and $^1$H NMR data show that this peroxide is bound in a symmetric fashion from both the standpoint of the peroxide ligand and that of the diiron unit, which leaves two reasonable possibilities for peroxide binding: $\mu$-$\eta^2$:$\eta^2$ and $\mu$-$\eta^1$:$\eta^1$ (Figure 7). The $\mu$-$\eta^2$:$\eta^2$ peroxide coordination would require rearrangement of the benzimidazole moieties of the HPTB ligand to the cis configuration and loss of both bound nitrate anions forming a 3+ cation, while the $\mu$-$\eta^1$:$\eta^1$ mode affords either a 1+ or a 2+ cation depending on the number of nitrates that remain coordinated. However, the fact that the energy of the peroxide charge-transfer band changes when carboxylates replace nitrates makes the displacement of both bound anions upon peroxide binding very unlikely.[63] Conductivity measurements in acetonitrile indicate

(57) Ahmad, S.; McCallum, J. D.; Shiemke, A. K.; Appelman, E. H.; Loehr, T. M.; Sanders-Loehr, J. *Inorg. Chem.* **1988**, *27*, 2230–2233.
(58) McCandlish, E.; Miksztal, A. R.; Nappa, M.; Sprenger, A. G.; Valentine, J. S.; Stong, J. D.; Spiro, T. G. *J. Am. Chem. Soc.* **1980**, *102*, 4268–4271.
(59) Okamura, M. Y.; Klotz, I. M.; Johnson, C. E.; Einter, M. C. R.; Williams, R. J. P. *Biochemistry* **1969**, *8*, 1951–1958.
(60) Armstrong, W. H.; Lippard, S. J. *J. Am. Chem. Soc.* **1984**, *106*, 4632–4633.
(61) Balch, A. L.; Chan, Y.-W.; Cheng, R.-J.; LaMar, G. N.; Latos-Grazynski, L.; Renner, M. *J. Am. Chem. Soc.* **1984**, *110*, 7779–7785.
(62) Suzuki, M.; Ueda, I.; Kanatomi, N.; Murase, I. *Chem. Lett.* **1983**, 185–188.

that, unlike the parent complex, which exhibits a conductivity value expected for a 2:1 electrolyte ($\Lambda_M$ = 240 $\Omega^{-1}$ cm$^{-1}$ mol$^{-1}$ for 8 × 10$^{-4}$ M complex in acetonitrile), the peroxide complex behaves like a 1:1 electrolyte ($\Lambda_M$ = 147 $\Omega^{-1}$ cm$^{-1}$ mol$^{-1}$ for 8 × 10$^{-4}$ M complex in acetonitrile).[64] We thus propose that peroxide binding appears to result in the replacement of the $\mu$-OH with a $\mu$-$\eta^1$:$\eta^1$ peroxide moiety with the retention of the basic ligand coordination around the dibridged dinuclear center (Figure 7a). This proposed structure for $[Fe_2(HPTB)(O_2)(NO_3)_2]NO_3$ is different from that proposed for the dioxygen adduct of $[Fe_2(N\text{-Et-HPTB})(OBz)](BPh_4)_2$,[27] which consists of a tribridged diferric core analogous to the 2+ cation in Figure 7b with benzoate replacing nitrate. The structural differences in the two peroxide complexes may be reflected in the subtle changes in their UV–vis, Raman, and Mössbauer parameters (Tables III and IV).

All of the diferric peroxide complexes studied thus far appear to favor peroxide bridge formation, and none of these complexes model the dioxygen-binding mode found for oxyhemerythrin.[8,26-28,56] Those capable of reversible dioxygen binding derive from monoferrous precursor complexes and presumably have trans $\mu$-$\eta^1$:$\eta^1$-peroxo coordination.[25,26] The diferric peroxide complexes derived from dinucleating ligands such as HPTB and HXTA are most likely to have cis $\mu$-$\eta^1$:$\eta^1$ peroxide coordination and appear incapable of reversible dioxygen binding. They are reactive toward organic substrates[29,30] and may thus more appropriately model the diiron–dioxygen interactions in ribonucleotide reductase and methane monooxygenase, diiron proteins that activate dioxygen.[4,10] A detailed study of the reactivity of the $[Fe_2(HPTB)(OH)(NO_3)_2](NO_3)_2$/peroxide complex toward organic substrates is in progress.

**Acknowledgment.** This work was supported by the National Institutes of Health through Grants GM-38767 (L.Q.) and GM-22701 (Eckard Münck), a predoctoral traineeship for B.A.B. (Grant GM-08277), and a postdoctoral fellowship for A.E.T. (Grant GM-12792), and by the E. G. Schleider Educational Foundation (C.J.O.). Beamline X9A at NSLS is supported by the National Biostructures PRT under NIH Grant RR-01633. We are grateful for Professor James Terner's assistance in preparing the isotopically labeled hydrogen peroxide and for Dr. Robert Kean's assistance in assembling the low-temperature resonance Raman equipment.

(63) Brennan, B. A.; Chen, Q.; Que, L., Jr. Unpublished results.
(64) Geary, W. J. *Coord. Chem. Rev.* **1971**, *7*, 81–122.

Contribution from the Department of Chemistry, University of Sofia, 1126 Sofia, Bulgaria, Institute of Applied Mineralogy, Bulgarian Academy of Sciences, 1000 Sofia, Bulgaria, and Institute of General and Inorganic Chemistry, Bulgarian Academy of Sciencies, 1040 Sofia, Bulgaria

# Chelating Modes of 3-Substituted 2,4-Pentanediones. Crystal and Electronic Structure of Bis(3-cyano-2,4-pentanedionato)cobalt(II)

Olyana Angelova,*,† Josef Macicek,‡ Michail Atanasov,§ and Galin Petrov†

*Received May 25, 1990*

Coordination modes of 3-substituted 2,4-pentanediones are considered with respect to the chemical nature of the substituent and the conformational flexibility of the ligand. Examples of additional and competitive coordination of the extra donor site(s) are given, and two different pathways for the structural rearrangement in such complexes are discussed. Accordingly, a new constitution of the acetylacetone cyanation intermediate product **4** in its Cu and Ni complexes is speculated. The 3D network structure of the title compound in which all functional groups are involved in coordination is determined ($C_{12}H_{12}CoN_2O_4$, tetragonal, space group $P4_2/n$, $a$ = 14.444 (1) Å, $c$ = 6.832 (2) Å, $D_x$ = 1.431 g cm$^{-3}$, $Z$ = 4, $R$ = 0.0217), and its solid-state electronic spectrum is analyzed in terms of the angular overlap model.

## Introduction

The structure and stability of 3-substituted 2,4-pentanedionato chelate complexes are influenced by the electron-withdrawing strength of the substituent to different extents.[1] For instance, nitro, cyano, and halogeno groups cause an electron density shift away from the central atom[2] and weakening of the coordinate bonds.[3] As a result, the prerequisites for the formation of additional (with preservation of the O,O-chelate; **1**) or competitive (toward a carbonyl group; **2**, **3**) coordination of the substituent are established.

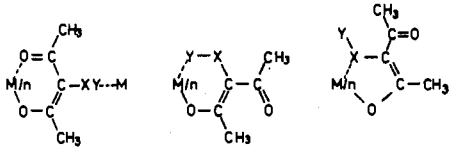

**1** **2** **3**

Type **1** intermolecular bonding is realized in the $[(NH_3)_5CoNCacacCr]^{4+}$ complex cation,[4] where NCacacH = 3-cyano-2,4-pentanedione (XY = CN). Recently, we reported the structure of $Cu(NCacac)_2$,[5,6] in which one of the cyano groups is linked to an adjacent copper atom. The presence of intramolecular additional coordination of the hexafluorobut-2-enyl substituent (XY = $CF_3C{=}CCF_3$) to iridium and rhodium atoms has been reported by Russell et al.[7]

**Scheme I**

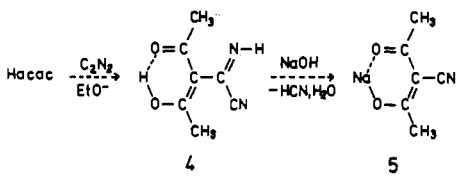

**4** **5**

† University of Sofia.
‡ Institute of Applied Mineralogy, BAS.
§ Institute of General and Inorganic Chemistry, BAS.

(1) (a) Tsiamis, C.; Cambanis, S.; Hadjikostas, C. *Inorg. Chem.* **1987**, *26*, 26. (b) Tsiamis, C.; Cambanis, S.; Jannakoudakis, A. D.; Theodoridou, E. *J. Electroanal. Chem. Interfacial Electrochem.* **1988**, *252*, 109.
(2) Sahai, R.; Verma, R. *J. Indian Chem. Soc.* **1981**, *58*, 640.
(3) Tanaka, M.; Shono, T.; Shinra, K. *Bull. Chem. Soc. Jpn.* **1969**, *42*, 3190.
(4) Balahura, R. J.; Johnston, A. J. *Inorg. Chem.* **1983**, *22*, 3309.
(5) Angelova, O.; Petrov, G.; Macicek, J. *Acta Crystallogr.* **1989**, *C45*, 710.
(6) Such bridging behavior of the cyanoacetylacetonato ligand was earlier reported by Thompson et al. from spectroscopic analysis of zirconium and titanium complexes: (a) Thompson, D. W.; Barrett, P. B.; Lefelhocz, J. P.; Lock, G. A. *J. Coord. Chem.* **1973**, *3*, 119. (b) Lock, G. A.; Thompson, D. W. *J. Chem. Soc., Dalton Trans.* **1980**, 1265.
(7) (a) Russell, D. R.; Tucker, P. A. *J. Chem. Soc., Dalton Trans.* **1975**, 1749. (b) Barlex, D. M.; Evans, J. A.; Kemmitt, R. D. W.; Russell, D. R. *J. Chem. Soc., Chem. Commun.* **1971**, 331.

0020-1669/91/1330-1943$02.50/0 